SciencePG
Science Publishing Group

Photo-thermal Conversion Efficiency of Textured and Untextured Aluminum Substrate Coated with Titanium Dioxide (TiO$_2$)-bound CuFeMnO$_4$ Absorber

Charles Opiyo Ayieko[1, *], Robinson Juma Musembi[1], Benard Odhiambo Aduda[1], Alex Ogacho[1], Pushpendra Jain[2]

[1]Department of Physics, University of Nairobi, Nairobi, Kenya

[2]Department of Physics, University of Botswana, Gaborone, Botswana

Email address:
opiyoc2006@yahoo.com (C. O. Ayieko)
[*]Corresponding author

To cite this article:
Charles Opiyo Ayieko, Robinson Juma Musembi, Benard Odhiambo Aduda, Alex Ogacho, Pushpendra Jain. Photo-thermal Conversion Efficiency of Textured and Untextured Aluminum Substrate Coated with Titanium Dioxide (TiO$_2$)-bound CuFeMnO$_4$ Absorber. *American Journal of Modern Energy*. Vol. 6, No. 1, 2019, pp. 9-15. doi: 10.11648/j.ajme.20200601.12

Abstract: The possibility of obtaining thermal energy from the sun for household bathing and washing has resulted to growth in market for solar thermal applications with new types of solar absorbers currently being investigated either to compliment or to replace existing ones. This study focuses on CuFeMnO$_4$ absorber paint by addressing aspects which have little attention regarding improvement of optical absorption for higher efficiency such as texturing the metal substrates on which to coat CuFeMnO$_4$ absorber paint. In this study, texturing was done controllably in order to match the incoming solar radiation wavelength and the surface topography and morphology. Textured and untextured aluminum sheets coated with titanium dioxide (TiO$_2$)-bound CuFeMnO$_4$ absorber paint were used to fabricate prototype flat plate solar thermal collectors. Titanium dioxide (TiO$_2$) was chosen here as binder to a spectrally selective CuFeMnO$_4$ absorber paint. The TiO$_2$-bound CuFeMnO$_4$ absorber paint was applied by a simple, cheap and up-scalable dip coating method over the aluminum sheets. The aluminum sheets were electro-chemically textured to enhance optical absorption and photo-thermal conversion efficiency for both the textured and untextured prototypes were compared. The efficiency characterization of the prototype collectors was done by measuring the global solar irradiance, fluid inlet, fluid outlet and ambient temperature. Both instantaneous and steady-state efficiencies were determined mathematically, and it was found that the prototype collector whose absorber plates were textured recorded higher instantaneous and steady-state efficiencies compared to the collector fabricated from untextured aluminum plates.

Keywords: Aluminum, Texturing, Conversion Efficiency, Solar Energy, (TiO$_2$)-bound, CuFeMnO$_4$

1. Introduction

Increase in human population accompanied by the energy-driven lifestyle has led to the search for more energy sources to complement the existing and established sources to sustain the high energy demands. Several options are being sought to extend the limited supply of energy. These include but not limited to; rationing, exploiting alternative energy sources to supplement the existing ones, and embracing energy saving practices for efficient utilization [1].

Solar photo-thermal energy is a promising and sustainable alternative energy source. When harnessed by ideal photo-thermal solar converters to obtain heat energy, it has a practical limiting efficiency of 84.4% [2]. By use of appropriate technologies and materials, solar energy can be harnessed using flat plate solar thermal collectors to complement the conventional energy sources that are often centralized and costly to access [3]. In heating applications, the most commonly used home appliances such as electrical water heaters are energy guzzlers and consequently expensive. However, household requirement of hot water can be significantly met using solar thermal energy by employing

solar thermal collectors [4].

Paint-based solar absorber has become cheap alternative to the more sophisticated surface treatment techniques such as electro-chemical, chemical and physical vapor deposited (PVD) coatings. This is because the absorber paint can be coated on substrates using simple and low-cost techniques such as spray coating or dipping [5]. Therefore paint-based solar absorber offers the opportunity to produce at large scale solar thermal collectors at a cheaper cost and simpler technology as opposed to the conventional electro-chemical, chemical and physical vapor deposited (PVD) coatings whose products were expensive and thus discouraging the use of solar energy as a renewable source.

The solar selective absorber paint (CuFeMnO$_4$) has recently been studied by [6] and found to register 0.94 of absorptivity and requires an optically optimum medium as a binder to a substrate. Titanium dioxide (TiO$_2$) is highly transparent in infrared region has low thermal emittance as found out by [7]. Further proof for suitability of TiO$_2$ is inferred from the work by [8] that studied Nb-TiO$_2$ cermet (ceramic-metal) for solar thermal application where the model and experimental analysis both registered spectral solar absorbance of 0.93 and thermal emittance of 0.09 which were favorable values for spectral selectivity.

Very little research has been done to advance the idea of surface morphology as a way of getting significant increase in absorption especially within specific wavelengths. A study by [9] just hints the importance of surface roughness but does not show tailor-made substrates or deposition techniques to achieve wavelength-specific surfaces treatments. It is until recently that a study by [10] of versatile roll-to-roll (R2R) process based on the anodization of aluminum foils for the controlled nano-texturing that the aspect of surface roughness was highlighted. This technique could treat substrates over large area with tunable surface topography. Such surfaces exhibit functional optical properties that can be optimized for particular applications.

This work, therefore, focused on CuFeMnO$_4$-paint while addressing aspects which have received little attention such as improvement of absorbance, α. The improvement of absorbance can be accomplished by employing surface texturing of metal substrates on which the absorber paint, CuFeMnO$_4$ is coated [11]; and by use of suitable infrared (IR) transmitting absorber paint binder to reduce thermal emittance [12].

1.1. Optical Characteristics of a Selective Solar Absorber

For a radiation incident on a thin film, the interaction between the medium and the radiation is described by equation (1) [13];

$$\tau(\lambda) + R(\lambda) + A(\lambda) = 1 \qquad (1)$$

where A is the spectral absorbance, R is the reflectance and τ is the transmittance.

For films coated on an opaque substrate, light transmitted through the film will be reflected back through the film.

Therefore, equation (1) can be rewritten as;

$$A(\lambda) = 1 - R(\lambda) \qquad (2)$$

1.2. Efficiency Characterization of Flat Plate Solar Thermal Collector

Flat plate solar thermal collector efficiency is characterized, under steady state conditions, by the parameters related in equation (3) and equation (4) [14];

$$\eta_i = \frac{Q_u}{A_c G_T} = \frac{F_R \left[G_T (\tau A)_{av} - U_L (T_i - T_a) \right]}{G_T} \qquad (3)$$

where A_c is the collector aperture area, G_T the global solar irradiance, Q_u, the useful energy gain, F_R, the collector heat removal factor, U_L, overall heat loss coefficient, τA transmittance–absorbance product of the cover glass, T_i, the inlet temperature and T_a, the ambient temperature.

$$\eta_i = \frac{m C_p (T_o - T_i)}{A_c G_T} \qquad (4)$$

where C_p, the specific heat capacity of the fluid, m is the mass flow rate and η_i, instantaneous collector efficiency and T_o, is the outlet temperature.

For a collector operating under steady state conditions, the F_R, τA, and U_L are nearly constant. Therefore, by inspection, equations (3) and (4) plots as a linear graph of efficiency versus heat loss parameter given as $(T_i\text{-}T_o)/G_T$ with the line intercept on the vertical axis giving the product $F_R (\tau A)$ and the slope of the line gives - $F_R U_L$. The maximum achievable efficiency using solar thermal collector is limited by Carnot efficiency [15].

2. Experimental Procedures

2.1. Texturing

Four concentrations of 60.0ml electrolyte were prepared by mixing 1.0M of perchloric acid (RFCL Limited, India) and mixed with ethanol in varying ratios of 1:0, 1:1, 1:2 and 1:3 by volume. The solutions were used for the texturing of different polished samples of aluminum. The temperature of the electrolyte during texturing was maintained below 10.0±0.5°C using an ice bath. Localized heating was guarded against during polishing, uniform distribution of heat in the electrolyte was ensured through continuous stirring using a magnetic stirrer.

Cylindrical graphite cathodes of dimension, 2.0cm in diameter and 10.0cm long were used for texturing. More than half of the length of the electrode was immersed in the electrolyte with polished aluminum surface of approximately 9.0cm^2 immersed for texturing at the anode. Direct current voltage of 30.0V was supplied for 30 minutes through the electrolyte from a DC voltage source which could deliver a maximum of 1.5 amperes (A). Figure 1 illustrates the set-up

for the texturing process.

To remove the fine particles of graphite deposited on the textured aluminum samples, the textured samples were first rinsed in distilled water for 3 minutes in a sonicator followed by rinsing in acetone for 3 minutes also in a sonicator. The rinsed samples were dried in air over hot plate at 40.0°C for 20 seconds and then kept in air-tight poly-ethane bags. The optimum result was achieved from the sample etched in acid-ethanol ratio of 1:2 which was subsequently used to build the textured prototype.
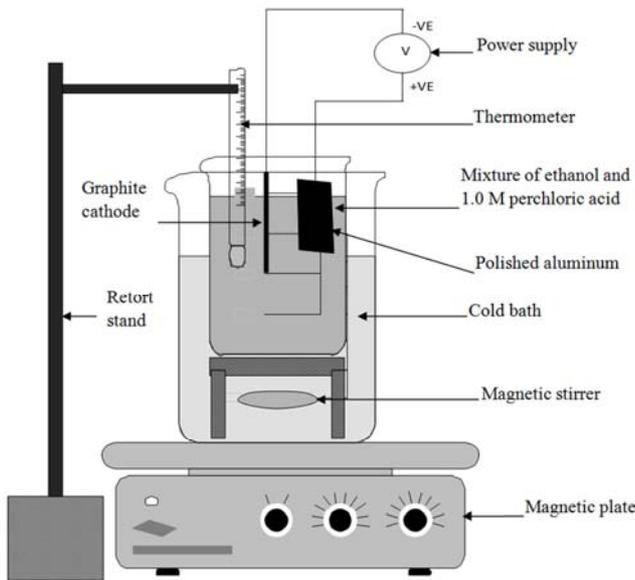

Figure 1. *Experimental set-up for texturing polished aluminum samples.*

For the fabrication of prototypes, aluminum plates of sizes 15.0×30.0 cm were annealed in air in a glass blowing unit at temperature of 450.0°C and textured in 10.0 litres of electrolyte of concentrations 1:2 of perchloric acid-to-ethanol ratio. The carbon electrodes used were proportionately large (10.0cm diameter by 37.0cm high) to ensure enough surface area of the cathode was exposed to the electrolyte for optimal texturing. A direct current of 25.0 A was applied across the electrolyte via the carbon and aluminum plate as cathode and anode electrodes, respectively for 30 minutes. The large currents were achievable by using power unit fitted with Variac which could deliver direct current and voltage outputs of 50.0 amperes and 25.0 volts.

2.2. Preparation of Titanium Dioxide (TiO₂ xH₂O) Solution and Thin Film Formation

One molar (1.0M) solution of titanium (IV) isopropoxide (99.7% pure) in isopropanol (99.7% pure) from Fluka Ltd was prepared and 28.0ml of the solution added gradually to 72.0ml of distilled water under vigorous stirring to disperse the white coagulates to form a homogenous mixture. The mixture was then stirred for 1 hour at 30.0°C to ensure complete hydrolysis. A molar (1.0M) solution of 5.0ml nitric acid was added dropwise to the mixture to speed up peptization and stirred at a temperature of 70.0°C for 7hrs so that ethanol could evaporate. This solution was left to cool to

room temperature, and it formed a stable clear solution of TiO_2 xH_2O where x is the molecules of water attached to TiO_2.

2.3. Preparation of TiO₂-bound CuFeMnO₄ Absorber Paint

Absorber paint solution was prepared by mixing 3.83g of $Mn(C_2H_3O_2)_4$, 1.37g of $FeCl_2$ and 2.30g of $CuCl_2$ in 50.0ml of ethanol under rigorous stirring at 70.0°C. A viscous solution resulted after 5 hours of stirring and was left to cool to room temperature. $CuFeMnO_4$ absorber paint was modified using TiO_2 as thermal emittance inhibitor. The titanium dioxide (TiO2)-bound $CuFeMnO_4$ absorber paint was prepared by mechanical mixing of ($CuFeMnO_4$) absorber paint and TiO_2 solution (as prepared in section 2.2). The mixture was dip-coated on the textured and untextured aluminum surfaces.

2.4. Fabricating Prototype Flat Plate Collectors

Two prototype flat plate solar thermal collectors with titanium dioxide (TiO_2)-bound $CuFeMnO_4$ prepared by dip-coating were made: one with textured surface and the other not textured. The textured plates prepared as per section 2.1 were dried in air and dip-coated with the absorber (TiO_2: $CuFeMnO_4$) and the coated plates subsequently annealed in air in an enclosed furnace for 1 hour at 400.0°C and thereafter allowed to cool in the furnace to room temperature. The annealed plates were attached to the fluid conduits of the prototypes by joining them together to form an area of $1m^2$ using rivets and thermally conductive adhesive (Clear silicon, Sparko USA Inc.). A panel of the joined plates attached to the fluid conduits was placed in a prefabricated metallic box. The metallic box with the panel of absorber plates was thereafter placed in another bigger metallic box that allowed an all-round space margin of 5cm. The 5cm space margin allowed for application of liquid thermal insulation (polyurethane) on the sides and the bottom of the box leaving the glazed top exposed for incoming solar radiation. The fluid conduits that were made from 1.25mm diameter copper tubing had two open ends to allow water in and out of the collector.
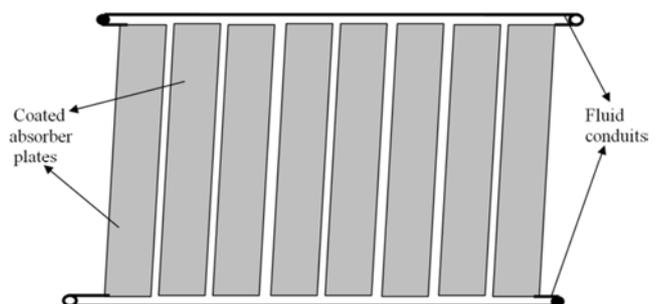

Figure 2. *A schematic diagram of an exploded view of the prototype absorber plate.*

2.5. Prototype Flat Plate Collector Efficiency Measurement

Figure 3 is a schematic diagram for the experimental set-up adopted for measurement of the efficiency. The set-up

ensured equal symmetry both on the left-hand side (textured) and right-hand side (untextured). This symmetry was considered in order to minimize variation in the path travelled by water hence equal volume reached both collector inlets at a time. The set-up further minimized errors due to varying inlet temperatures that could affect comparison of calculated efficiency values of the collectors. Apart from the set-up occupying a small space and it was also financially economical for our study since just one tank was used as opposed to two tanks.
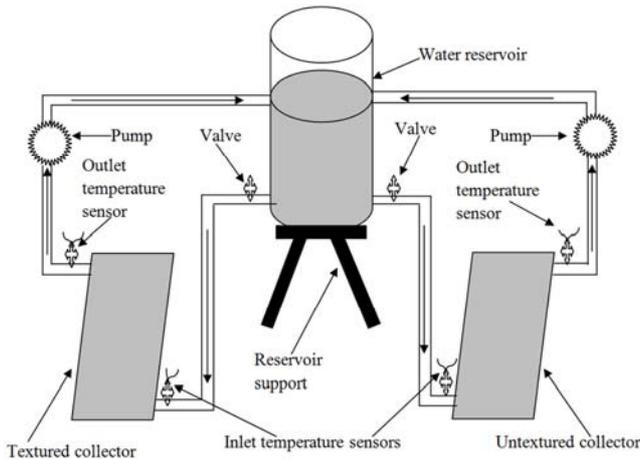

Figure 3. *A schematic diagram of the experimental set-up for collector efficiency measurement.*

The instantaneous collector efficiency was ascertained by carrying out tests with the following parameters determined: fluid mass flow rate (5.0g per second), global solar irradiance at the plane of the collector measured using pyranometer (Model HT 303), ambient temperature, and fluid inlet and outlet temperatures measured using type-K thermocouple sensors. The temperature data was collected using a plug and play data logger (DATAQ-DI-v1.61) which uploaded the data into a computer for analysis using EXCEL software.

The collector parameters used were measured simultaneously for both textured and untextured for a period of 1 hour and the values for global irradiance, ambient temperature and inlet temperature averaged to closely simulate steady state conditions. The efficiency for the textured and untextured surfaces both in steady state and instantaneous conditions were calculated and graphically presented in section 3.0. The other values that were used for the calculation of efficiency were specific heat capacity for water which was taken to be 4200J/Kg °C and the collector aperture area which was 1.0±0.1m^2 being the approximate area covered by the active absorber plate surface.

3. Results and Discussion

3.1. Efficiency of Prototype Flat Plate Collector

Figure 4 is a plot of instantaneous collector efficiencies at varying solar radiation levels but with longer sunshine

duration at around 300W/m^2 where most of the data were clustered. It is evident that the collector fabricated from the textured plates has high instantaneous efficiency, η_i, for all levels of solar radiation as is evident from an upward shift in the graph representing the textured data as opposed to that of untextured. The efficiency ranged between 0.10 and 0.40 for the untextured surface, with a mean value of 0.20 while textured surface realized an efficiency range of 0.50 to 0.85 with a mean value of 0.60.

As the level of irradiance increased from 300W/m^2 towards 900W/m^2 the efficiency decreased. The decrease can be explained by the fact that a unity increases in irradiance does not produce a corresponding proportional unity increase in temperature change. This trend of the decrease in efficiency as irradiance increases from a stable level is as a result of the inverse relation expressed in equation (4) restated in this section [14]. It is inverse relation in the sense that a bigger change in solar irradiance, G_T corresponds to a disproportionately smaller change in the difference between inlet and outlet collector temperatures $(T_o - T_i)$.

$$\eta_i = \frac{mC_p(T_o - T_i)}{A_c G_T} \qquad (4)$$

The scattered points towards higher irradiance levels (>400W/m^2) also depict a situation where higher levels of irradiance lasted a very short periods within the 1-hour data collection duration when the collector was exposed to the sun.
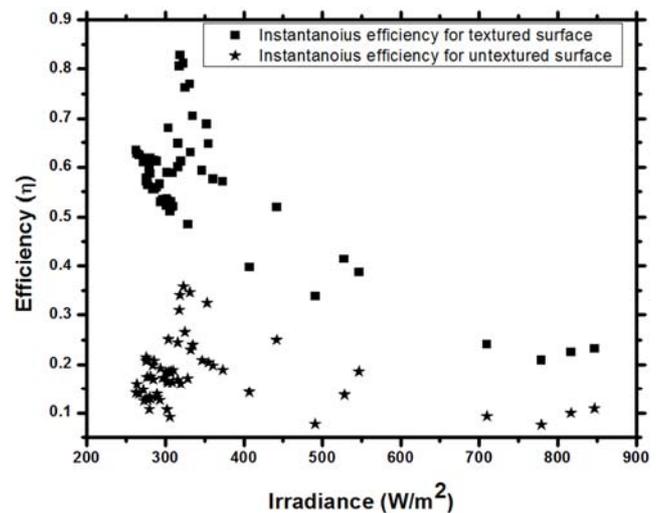

Figure 4. *Instantaneous efficiency of prototype solar thermal collector at various solar radiation levels peaking at 300W/m^2.*

Figure 5 shows the relation between instantaneous efficiency, η_i, and total solar irradiance but with long sun shine duration dominantly around 800W/m^2 as opposed to lower irradiance level of 300W/m^2 in Figure 4 The textured surface likewise registers higher steady state efficiencies ranging between 0.50 and 0.80 compared to a lower range of 0.20 and 0.40 for untextured surface and the upward shift in instantaneous efficiencies just as in

Figure 4 is evident from Figure 5. The inverse relation of efficiency with solar irradiance as shown by equation (4) and the less responsiveness of temperature change with increase in solar irradiance are also noticed as in the case for Figure 4.
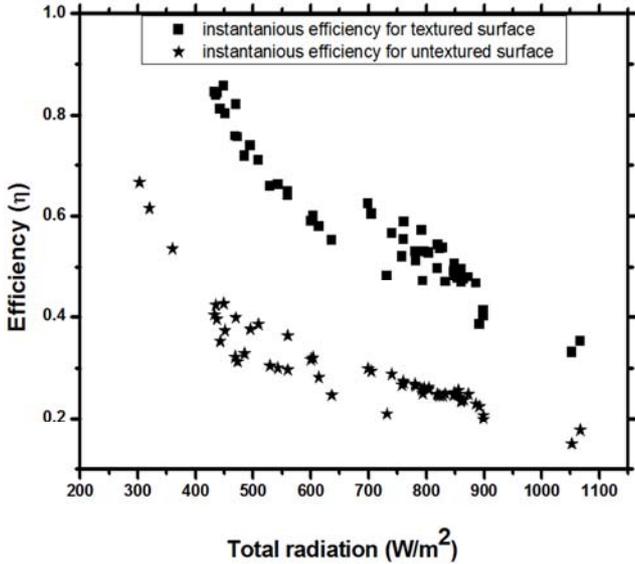

Figure 5. Instantaneous efficiency of prototype solar thermal collector at various solar radiation levels peaking at 800W/m².

The trend of higher efficiency for textured surface compared to that of the untextured surface was also observed for the prototypes when exposed to solar irradiance long period dominantly at 850W/m² (Figure 6). The textured surface recorded efficiency range between 0.65 and 0.80 as opposed to the untextured that registered between 0.20 and 0.275. Since solar irradiance remained fairly constant between 800W/m² and 900W/m², efficiency did not change drastically as seen in Figure 4 and Figure 5.
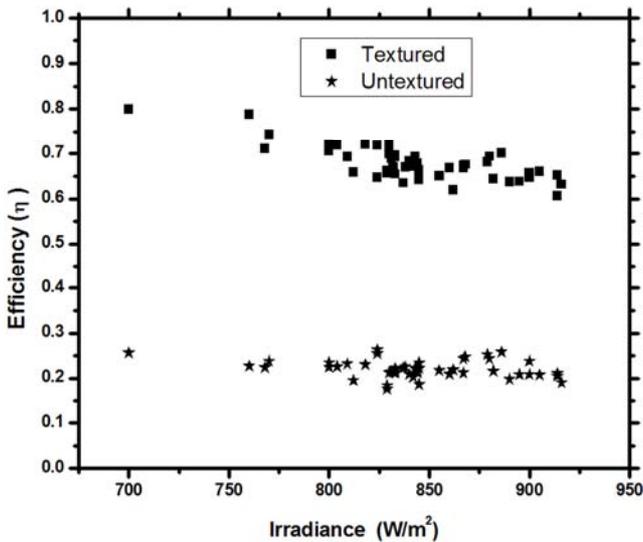

Figure 6. Instantaneous efficiency of prototype solar thermal collector at various solar radiation levels at irradiance peaking at 850W/m².

A plot of efficiency against temperature difference

between the inlet temperature and the outlet temperature divided by the energy input (300W/m², 700W/m² and 850W/m²) is shown in Figure 7. The upper graphs represent efficiencies for the textured surface while the lower ones represent efficiencies for the untextured surface. The straight-line graphs are the best line of fit of the data points for both textured and untextured surface exposed to different levels of irradiation (300W/m², 700W/m² 850W/m²). Based on equation (5) [14];

$$\eta_i = \frac{Q_u}{A_c G_T} = F_R (\tau\alpha) - \frac{F_R U_L (T_i - T_a)}{G_T} \qquad (5),$$

data points for steady-state efficiencies were plotted and linear fit of the points derived as shown in Figure 7. Due to variation of weather conditions perfect linear plot is not achievable and therefore the data points are fitted linearly.
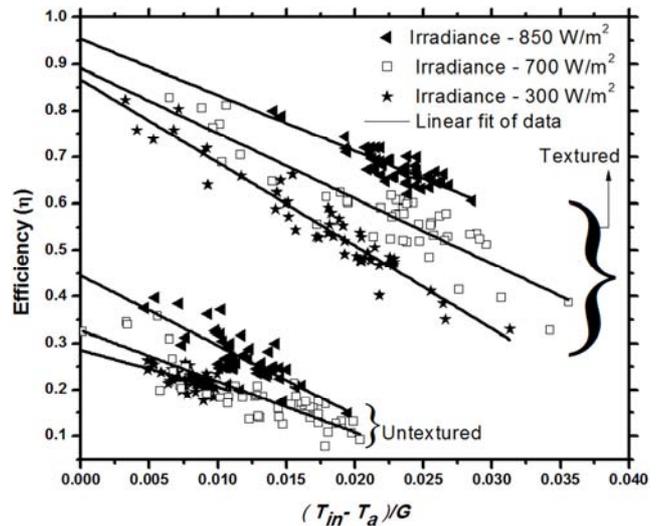

Figure 7. Steady-state efficiency textured and untextured surface of prototype solar thermal collector taken at three values of average total solar irradiance. T_{in} is the inlet temperature; T_a is the ambient temperature and G is the total irradiance in W/m².

Each linear fit has an equation from which the gradient was derived and the y- intercept read out. Solar thermal collector performance analysis calls for knowledge of two physical parameters namely; the heat removal factor (F_R) and overall heat loss coefficient (U_L) derived from the y-intercept and gradient respectively. The heat removal factor indicates the ratio of actual energy transferred to working fluid to that of the energy available to the absorber surface. In our study, low iron content glass was used as a single cover and according to [14] window glass (5 mm thick) cover has typical transmittance-absorbance (τA) value of 0.90. Table 1 presents equation of each linear curve and the corresponding overall heat loss coefficient and heat removal factor as derived from Figure 7.

Textured surfaces recorded high heat removal factors compared to untextured surfaces. It is worth noting from all the graphs showing efficiency (Figures 4, 5, 6 and 7) that the level of efficiency is not dictated by the irradiance level and

textured surface gives higher efficiency than untextured surfaces. The increase in efficiency for textured surface is attributed to increased absorption of light rays due to multiple reflections and increased surface area. The efficiency could not reach unity (1) because of the reflective loses of irradiance of the glass cover surface coupled with radiative and convectional heat leakages. The high values of efficiency noted of up to 0.85 for the textured surface can be justified from the Carnot's efficiency limit if the collector is

Carnot's engine. The Carnot's efficiency relation is mathematically stated as below [15].

$$\eta_c = 1 - \frac{T_l}{T_h} \qquad (6)$$

where T_h and T_l are output (high) and input (low) temperatures respectively.

Table 1. *Equations of the linear-fit curves and corresponding and heat removal factor (F_R) and overall heat loss coefficient (U_L) with a calculated error of ±0.1.*

	300W/m^2	700W/m^2	850W/m^2
Textured Surface	$y = -17.624x + 0.867$	$y = -13.997x + 0.891$	$y = -11.996x + 0.950$
	$F_R = 0.963 \pm 0.100$	$F_R = 0.995 \pm 0.100$	$F_R = 1.037 \pm 0.100$
	$U_L = 18.30 \pm 0.10$	$U_L = 14.07 \pm 0.10$	$U_L = 11.57 \pm 0.10$
Untextured Surface	$y = -7.997x + 0.285$	$y = -9.953x + 0.311$	$y = -14.732x + 0.442$
	$F_R = 0.380 \pm 0.100$	$F_R = 0.415 \pm 0.100$	$F_R = 0.589 \pm 0.100$
	$U_L = 21.04 \pm 0.10$	$U_L = 23.98 \pm 0.10$	$U_L = 25.01 \pm 0.10$

Considering that the water being heated is flowing in conduits which are fused on the absorber plates which are at temperature T_h, the separation between the water and absorber plate is so small and therefore T_h may be considered as the absorber plate temperature. From the relation in equation (6) and if the difference in output temperature and input temperature is large and $T_h > T_l$ as is usually the case for solar thermal collectors, the Carnot efficiency which is the limiting efficiency gives high values as opposed to when the difference is small. Therefore, solar thermal collectors are usually very efficient for heat conversion. These high efficiency values were also observed by [14] while making a comparison between values of efficiency for different types of solar thermal collectors at different values of solar irradiance under steady state who found values as high as between 0.70 to 0.80.

4. Conclusion

The study was set out to compare the photothermal efficiency of the plain, untextured aluminum surface with that of the etched/textured aluminum surface for solar thermal collector applications. The prototypes worked well, and the dipping technique adopted for coating the absorber was up-scalable for large surfaces. The concept of up-scalability was also evident for electro-chemical etching/texturing and gave the prospects of production for the market. The higher efficiencies realized with the textured surfaces is an indication that for a given flow rate, higher fluid outlet temperatures are attainable if compared with the untextured surface. Electrochemical etching/texturing should therefore be considered a feasible technique as an alternative to solar collector concentrators. Concentration through etching/texturing comes about when the pores on the textured surface multiply reflects solar radiation and the pores themselves increases the surface area of interactions with the rays. Multiple reflections and

increase in surface area results in high values of heat removal factor for the textured surfaces as compared to the untextured ones. The local temperatures of the absorber surface for textured prototype were higher than those of the untextured surfaces resulting to higher overall heat loss coefficients for the textured surfaces compared to the untextured surfaces. The collector fabricated from the textured plates has high steady state and instantaneous efficiency. Further the rate of change of irradiance level does not give rise to equal and proportionate change in temperature.

Acknowledgements

References

[1] Hankins, M. (1995). Small Solar Electric Systems for Africa. Motif Creative Arts, Ltd, Kenya. 61-65.

[2] Bermel, P., M. Ghebrebrhan, W. Chan, Y. X. Yeng, M. Araghchini, R. Hamam, C. H. Marton, K. F. Jensen, M. Soljacic, J. D. Joannopoulos, S. G. Johnson, and I. Celanovic (2010). Design and global optimization of high-efficiency thermo-photovoltaic systems, Opt. Express, 18, 314–334.

[3] Carley, S. (2009). Distributed generation: an empirical analysis of primary motivators. Energy Policy, 37, 1648-1659.

[4] El Bassam, N. (2017). Technologies and Options of Solar Energy Applications in the Middle East. In Water, Energy & Food Sustainability in the Middle East (pp. 193-221). Springer International Publishing.

[5] Perednis, D., & Gauckler, L. J. (2005). Thin film deposition using spray pyrolysis. Journal of electroceramics, 14 (2), 103-111.

[6] Tulchinsky, D., Uvarov, V., Popov, I., Mandler, D., & Magdassi, S. (2014). A novel non-selective coating material for solar thermal potential application formed by reaction between sol–gel titania and copper manganese spinel. Solar Energy Materials and Solar Cells, 120, 23-29.

[7] Ayieko, C. O., R. J. Musembi, S. M. Waita, B. O. Aduda, P. K. Jain (2012). Structural and Optical Characterization of Nitrogen-doped TiO2 Thin Films Deposited by Spray Pyrolysis on Fluorine Doped Tin Oxide (FTO) Coated Glass Slides. International Journal of Energy Engineering, 2 (3), 67-72.

[8] Wäckelgård, E., Mattsson, A., Bartali, R., Gerosa, R., Gottardi, G., Gustavsson, F.,... & Rivolta, B. (2015). Development of W–SiO2 and Nb–TiO2 solar absorber coatings for combined heat and power systems at intermediate operation temperatures. Solar Energy Materials and Solar Cells, 133, 180-193.

[9] Cuomo, J. J., J. F. Ziegler, J. M. Woodall (1975). A new concept for solar energy thermal conversion, Appl. Phys. Letters, 26 (10), 557-560.

[10] Min H. L., N. Lim, D. J. Ruebusch, A. Jamshidi, R. Kapadia, R. Lee, T. J. Seok, K. Takei, K. Young Cho, Z. Fan, H. Jang, M. Wu, G. Cho, A. Javey (2011). Roll-to-Roll Anodization and Etching of Aluminum Foils for High-Throughput Surface Nanotexturing, Nano Lett., 11, 3425–3430.

[11] Zeng, L., Yi, Y., Hong, C., Liu, J., Feng, N., Duan, X., B. A. (2006). Efficiency enhancement in Si solar cells by textured photonic crystal back reflector. Applied Physics Letters, 89 (11), 11111.

[12] Nahar, N. M. (2017). Selective coatings on flat-plate solar collectors. International Energy Journal, 3 (1).

[13] Duffie, J. A. and Beckman, W. A. (2006). Solar Engineering of Thermal Processes, third ed. Wiley, USA, 78-84.

[14] Kalogirou, S., (2004). Solar thermal collectors and applications, Prog. Energy Combust. Sci., 30 (3), 231–295.

[15] De Vos, A. (1985). Efficiency of some heat engines at maximum–power conditions. American Journal of Physics, 53 (6), 570-573.